CT Angiography Technique: Contrast Medium Dynamics, Low-Tube-Voltage, and Dual-Energy Imaging

Richard Hallett[1,2], Lior Molvin[1], Dominik Fleischmann[1]

High-quality, consistent CT angiography (CTA) can be achieved with optimized CTA protocol design. Careful coordination of IV contrast medium (CM) administration and CT scanner protocol ensures CTA quality. In this chapter, we discuss rational methods to design CM injection protocols and coordinate these with robust CT scan acquisition. We also discuss the benefits and limitations of low-tube-voltage and dual-energy scanning for cardiovascular imaging.

Since its introduction in the 1990s [1], CTA has changed the paradigm for the diagnosis of cardiovascular disease and created a new management strategy for many cardiovascular disease processes. CTA uses bolus injection of IV CM to provide robust enhancement of vascular structures in the vascular territory of interest. Optimal CTA results require thoughtful matching of CM injection and image acquisition protocols. As CT scanner technology has evolved, substantially shorter scanning times have become possible, making precise tailoring of injection protocols and scan acquisition more important than ever. CT tube and detector advances have allowed routine imaging at lower tube voltages and have also been exploited to produce dual-energy CT (DECT) acquisitions. Enhanced options for improved image quality, radiation dose reduction, and dynamic imaging have become available [2].

The goal of this chapter is to provide the basic tools to design rational CM injection and CT scan acquisition protocols for cardiovascular CTA. We will review CM dynamics, discuss optimization of timing for CT acquisition, and review the use of low-tube-voltage and dual-energy techniques in cardiovascular CT.

Contrast Medium Considerations

Currently used radiographic contrast media are water-soluble derivatives of symmetrically iodinated benzene. For IV injection, typically nonionic CM is used, because these agents result in fewer adverse reactions and, at injection rates typical for CTA, less acute nausea and vomiting than ionic CM [3, 4]. Pharmacologically, iodinated CM is an extracellular fluid marker and, after injection, is rapidly distributed between intravascular and extracellular interstitial spaces. It is important to remember that vascular enhancement and organ enhancement are affected by different pharmacokinetics. Vascular enhancement depends on the relationship between iodine flow rate (milligrams of iodine per second) and cardiac output (liters per minute), whereas solid organ enhancement depends on the relationship between total iodine dose (milligrams of iodine) and total volume of distribution (body weight in kilograms). These differences form the rationale for current CM injection protocols.

Early Contrast Medium Dynamics

Figure 1 schematically illustrates early CM dynamics in an arterial segment. When a short bolus of CM is injected, an enhancement response is seen in the vessel of interest. The time needed for the CM to arrive in the vessel of interest is referred to as the CM transit time (t_{CMT}). The peak enhancement response is called the "first-pass" effect. After CM is distributed to the vascular and interstitial compartments, a portion of the CM reenters the right heart, which is called "recirculation." Both first-pass and recirculation effects occur during the timeframe relevant to CTA acquisition; therefore, both contribute to observed vascular enhancement. A longer CM injection (e.g., an injection protocol for CTA) can be viewed as the sum of multiple sequential short bolus injections [5]. Because the recirculation phase CM bolus curve overlaps with subsequent first-pass CM bolus curves, the result is that the cumulative enhancement curve is the sum (time integral) of each individual enhancement response curve. More simply, when CM is injected IV over 15 seconds or more, the observed arterial enhancement will continuously rise until the end of the CM injection and then rapidly fall. This observation can be exploited to optimize CM injection and scanning protocols. Note also that the resultant enhancement profile is not a plateau (a common misconception), although near-plateau enhancement curves can be approximated by using biphasic (or multiphasic) injection protocols [6].

Individual Contrast Medium Responses

The overall response to CM injection is governed by the early CM dynamics principles discussed earlier. However, individual patient and physiologic parameters affect observed contrast enhance-

[1]Department of Radiology, Cardiovascular Imaging Division, Stanford Hospital and Clinics, 300 Pasteur Dr, Grant Bldg, S-072, Stanford, CA 94305. Address correspondence to R. Hallett (hallett@stanford.edu).

[2]Northwest Radiology Network, Indianapolis, IN.

ment. Observed arterial enhancement varies significantly—up to a factor of 3—between individual patients even in those with normal cardiac output [7]. Even when accounting for patient size, the difference can still be a factor of 2 [8]. Adjustments to injection volume and flow rate are needed and can improve, but not eliminate, CM enhancement variability. Cardiac output is inversely related to first-pass arterial enhancement: More blood ejected per heartbeat means more dilution of CM [9]. The result is lower observed enhancement at high cardiac output (and vice versa). Likewise, central blood volume is inversely related to enhancement; however, unlike cardiac output, central blood volume is affected more by changes in recirculation effects [10]. Cardiac output and central blood volume measurements are typically not clinically available to the imager, but these parameters generally correlate with body weight. Therefore, body weight can be used to adjust injection protocols. The Valsalva effect is a physiologic state that impacts CM dynamics in two ways: by promoting a rush of unopacified blood from the inferior vena cava (resulting in washout of CM from the pulmonary arteries on examinations performed for suspected pulmonary embolus [11]) and by causing early arterial enhancement related to transient right-to-left shunting across a patent foramen ovale [12].

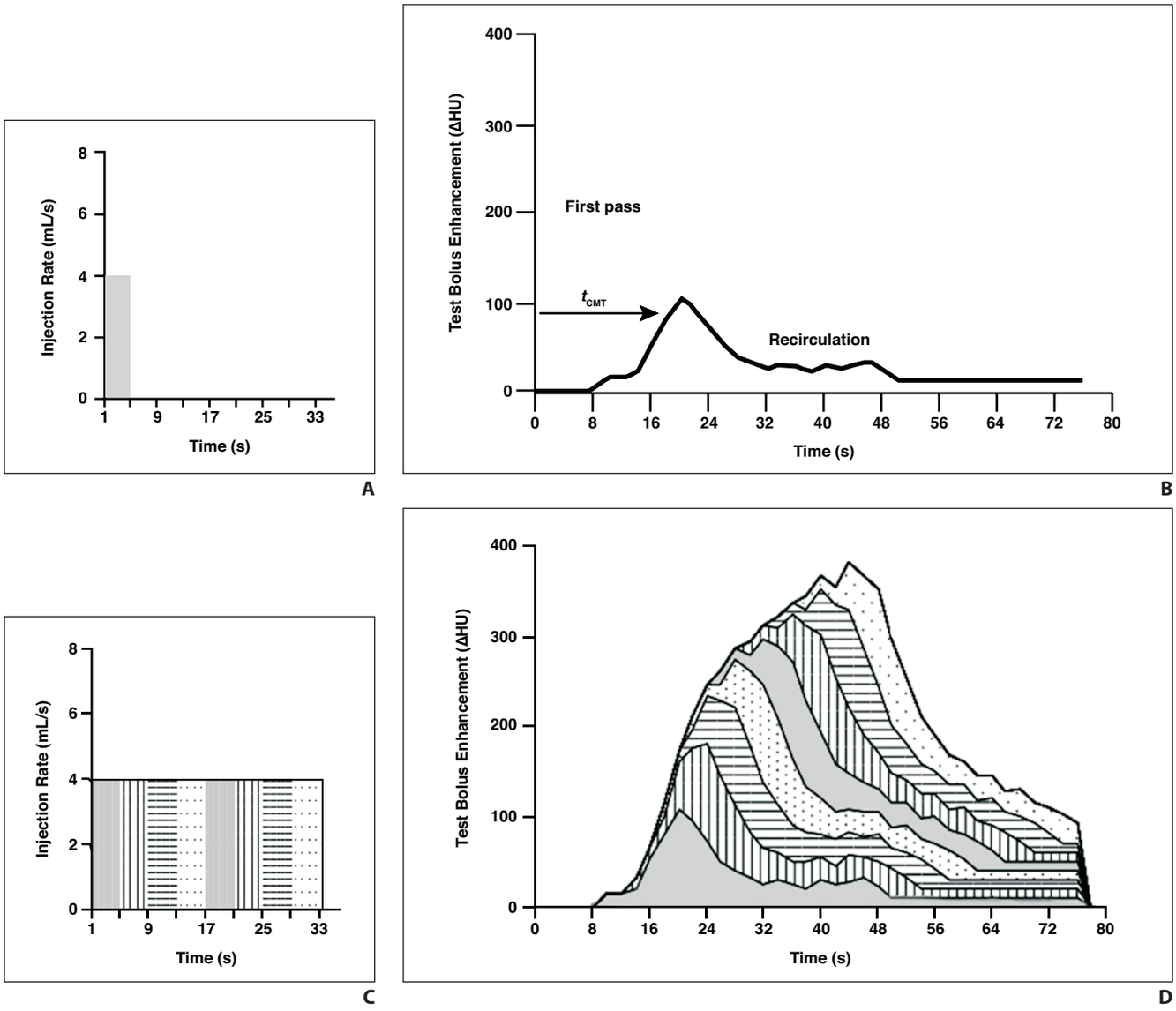

Fig. 1—Early contrast medium (CM) dynamics. (Adapted by permission from Springer Nature Customer Service Centre GmbH: Springer Nature *European Radiology*, Present and Future Trends in Multiple Detector-Row CT Applications: CT Angiography, Dominik Fleischmann, © 2002)
A and **B,** Graph shows time for injection of 16-mL CM test bolus at rate of 4 mL/s (**A**), and corresponding test bolus enhancement curve (**B**) shows cumulative arterial enhancement. In **B**, tail of enhancement results from recirculation effects related to CM reentering right heart, and CM transit time (t_{CMT}, *arrow*, **B**) is time from beginning of injection until CM arrives in area of interest.
C and **D,** Graph shows prolonged injection of CM test bolus (128 mL of CM [eight 16-mL boluses] at rate of 4 mL/s) (**C**), and corresponding test bolus enhancement curve (**C**) shows cumulative arterial enhancement. Because of asymmetric shape of test enhancement curve (shown in **B**) from recirculation effects, observed arterial enhancement for prolonged injection (**C**) increases continuously over time (**D**); there is no enhancement plateau. Different patterns illustrate each of eight boluses.

Another factor that must be considered is the fact that large or diseased vascular territories do not fill instantaneously; indeed, even the coronary tree needs several heartbeats to completely fill. The capacitance or disease extent in a particular territory is usually not known in advance and is often a reason for performing the examination. In particular, extensive lower extremity occlusive disease can result in significant prolongation of CM transit times. Therefore, when designing injection and scanning protocols for CTA, building in sufficient injection duration to allow filling of these vascular territories is important to ensure consistent results. When the injection duration is increased, the scanning delay must be increased proportionally to allow imaging of all CM given at the peak of the CM injection curve.

To summarize this information: early CM dynamics is governed by four rules [5]. The first rule is that arterial enhancement is directly proportional to iodine injection rate (milligrams of iodine per second). The second rule is that arterial enhancement increases in a cumulative fashion for the full duration of CM injection (no plateau). The third rule is that arterial enhancement is inversely proportional to cardiac output and circulating blood volume, which can be approximated by body weight. The fourth rule is that large or diseased vascular territories do not fill instantaneously.

Contrast Timing for CT Angiography Acquisition

In the early days of MDCT, table speed was a limiting factor for CTA image acquisition [13]. With current state-of-the-art scanners, table speeds can reach 737 mm/s, thus potentially exceeding expected blood flow velocity in many vascular territories [14]. Therefore, in many instances, it is advantageous to slow down the scanner to allow the entire vascular territory to fill. Appropriate matching of CM injection and CT acquisition protocols is necessary to produce high-quality, consistent CTA examinations.

CT Acquisition Speed

Modern CT acquisition speeds are not a major limiting factor for most CTA examinations. Faster acquisition speed reduces motion artifacts and may allow use of less CM, but this relationship is not directly proportional. To design rational cardiovascular CT protocols, it is important to be able to calculate the acquisition speed of the CT scanner so that appropriate matching of scanning time and CM injection profile can be performed.

For helical acquisitions, the scanning time can be determined as follows:

$$\text{scanning time} = \frac{\text{anatomic coverage [in millimeters]}}{\text{number of rotations}} \times \text{gantry rotation time},$$

where the number of rotations is calculated as follows:

$$\text{number of rotations} = \frac{\text{anatomic coverage [in millimeters]}}{\text{detector bank width [in millimeters]} \times \text{pitch}}.$$

The scanning time for a particular territory can therefore be maintained as constant (e.g., 10 seconds) by iteratively changing the gantry rotation time. Some vendors' software provides direct prescription of scanning time with automatic adjustment of other parameters; other platforms require interactive adjustment of parameters by the user. By keeping scanning time fixed, only the necessary CM dose and rate (depending on patient size) is needed to create a basic injection and scanning protocol tailored to the individual patient.

For prospective ECG-synchronized acquisitions (step-and-shoot mode), the scanning time is equal to the gantry rotation time if the *z*-axis scanning length is less than the detector bank width. For large-volume acquisitions, scanning times for each portion should be added to interscan times (for table movement and ECG triggering) to determine the total scanning time.

Note that it is important to understand the difference between scanning time and temporal resolution: the former represents the time needed to scan the entire volume of interest, and the latter represents the time needed to acquire projection data for one CT image. For single-source scanners, temporal resolution is approximately half the gantry rotation time, whereas for dual-source scanners the temporal resolution can be as short as one-quarter of the gantry rotation time.

There is no single correct or perfect injection and scanning protocol. We strive for practical, easy-to-use protocols that deliver consistent, reproducible enhancement over a large range of patient sizes and disease states. Building on the principles that we have discussed, an example injection and scanning protocol for body CTA is as follows [15]: scanning time, 10 seconds; injection duration, 18 seconds; CM injection rate, weight based (e.g., 5 mL/s for 75-kg patient = 90 mL); scan timing, automated bolus triggering to territory of interest; scanning initiation, 8 seconds after CM arrival.

A scanning time of 10 seconds is slow for current state-of-the-art scanners; however, nearly all currently available scanners can acquire CTA images of the abdomen and pelvis (and of the chest if needed) in this timeframe. Further, the 8 seconds of additional injection duration and scanning delay allows filling of aneurysmal or diseased vascular segments sufficiently. Adjustments in CM injection rate and CM volume can be made by direct calculation (e.g., milliliters per kilogram) or by weight groups for ease of use. Keeping injection duration and scanning time constant (vendor-dependent: by changing pitch or gantry rotation time or by directly entering these data on the scanner console) simplifies planning, because patient weight is the only variable affecting CM dose and CM injection rate between patients. It is important to note that we recommend using a saline chaser after CM injection—administered for at least 5 seconds at the same injection rate as that used for CM—to improve bolus integrity and decrease potential perivenous streak artifacts.

CT Scanner Technology: Low-Tube-Voltage and Dual-Source Imaging

Current Scanner Technology

A complete discussion of current CT scanner technology is beyond the scope of this chapter. However, it can be stated that advancements in CT tube and detector technology have allowed the modality to keep pace with and expand clinical applications. As gantry rotation speeds have increased, generators capable of higher photon output have been developed to sustain adequate image quality in high-temporal-

resolution environments. Current CT tubes have x-ray power ratings of up to 120 kW and available tube currents of 1300 mA per tube. These parameters not only support fast acquisitions with high temporal resolution but also use lower tube voltage in most patients and allow improved imaging of obese patients. Many scanners also allow rapid electronic flipping of the x-ray focal spot in the *z*-axis, producing two separate projections or "slices" for each detector row (and thus reported as double the number of detector rows). For example, manufacturers often report a scanner having 128 detector rows that uses *z*-focal spot flipping as "256-slice CT."

Low-Tube-Voltage Imaging

As we discussed earlier, powerful x-ray tubes of modern CT scanners allow the use of lower peak tube voltage compared with previous generations of scanners that use the standard 120 kVp. At lower tube voltage, photon absorption by iodine (as contained in iodinated CM) is increased as the energies approach the k-edge of iodine (i.e., 33.2 keV). This translates into higher attenuation values and greater observed contrast enhancement of vessels and organs [16]. In general, the attenuation of iodine increases by approximately 25% in each "step" from 120 to 100 kVp, 100 to 80 kVp, and 80 to 70 kVp (Table 1). As a result, the volume of CM needed to achieve similar attenuation decreases proportionally if image noise can be maintained. Note that to maintain consistency in scanning protocol design, it is helpful to adjust other scanning parameters accordingly (e.g., injection duration, scanning time, built-in delays).

Imaging at lower tube energies results in a larger fraction of photons absorbed by tissues, resulting in increased image noise. Therefore, an increase in x-ray tube current (milliamperes) is needed to maintain constant image noise. In general, tube current should be increased 30–50% for each tube voltage step discussed earlier. Other strategies that can be used include prolonging the gantry rotation time or decreasing the pitch (to increase the tube current–time product [milliampere-seconds]). All of these techniques can decrease image noise, albeit at the expense of increasing patient dose. In recent years, the introduction of iterative reconstruction (IR) techniques has allowed decreases in image noise without increasing patient dose; however, high levels of IR may result in visually disconcerting images—described as "waxy," "oversmoothed," and "blotchy" [17]—with reduced image quality even if the signal-to-noise ratio (SNR) or contrast-to-noise ratio (CNR) suggests otherwise [18]. Given that patient size has a nonlinear effect on x-ray absorption, selection of an optimized tube voltage for a given patient may not be intuitive. Automated tube voltage selection software has been developed that allows optimization of tube voltage based on data contained in the CT topogram (i.e., the so-called "digital radiograph") [19]. Newer scanners have built-in CNR calculators that allow dose reduction and kilovoltage optimization based on the examination type (e.g., cardiac or vascular territory, solid-organ imaging, and so on) and on individual patient characteristics [20, 21]. A combination of these techniques is optimal to achieve a balance of image quality and patient dose.

Low-tube-voltage imaging has potential disadvantages. Higher tube current requirements for low-tube-voltage imaging require a larger focal spot size, resulting in decreased spatial resolution [22], potentially limiting measurement accuracy and reproducibility. Beam-hardening artifacts and blooming artifacts related to calcification and metallic implants (e.g., stents, wires, prostheses) can be more pronounced. As a result, postprocessing and visualization techniques that create additive image noise across a slab (e.g., maximum intensity projection) can become more difficult to reliably assess.

TABLE 1: Iodine Attenuation at Different Tube Voltage Settings Compared With Iodine Attenuation at 120 kVp

Tube Voltage	Change in Iodine Attenuation Compared With Iodine Attenuation at 120 kVp
140 kVp	↓ 25%
120 kVp	Reference
100 kVp	↑ 25%
80 kVp	↑ 50%
70 kVp	↑ 70%

Note—Down arrow indicates a decrease, and up arrow indicates an increase.

Dual-Energy Technology

The introduction of DECT technologies has allowed exploration of new areas in vascular imaging. All major CT manufacturers currently have developed scanners that can generate DECT images [23]. Dual-source CT (DSCT) [24] consists of two x-ray tubes positioned at an approximate 90° angle that rotate together but can function independently at different tube voltage settings. These scanners can also use a rapid shuttle system to scan and rescan the same anatomic area with different tube voltage settings. Single-source CT systems with rapid tube voltage switching [25] and dual-layer spectral detectors [26] have been developed. Development of photon-counting CT detectors using cadmium-based detector materials allows energy-specific measurements and rejection of electronic noise, resulting in robust energy discrimination. However, photon-counting CT technology is limited by loss of counts and potential detector paralysis related to pile-up effects at clinical photon rates [27]. The distribution of a photon's energy across multiple detector pixels (i.e., charge sharing) also limits current photon-counting detectors [28]. Photon-counting CT technology has not yet reached commercial implementation.

Regardless of the acquisition technique, the end result of DECT image acquisition is the generation of two independent datasets at different tube voltage settings. By using the spectral behavior of elements in the two datasets (e.g., 140 and 80 kVp), the inherent spectral differences between tissues with higher (iodine) and lower (calcium) atomic number can be exploited. Decomposition of tissues (tissues with iodine, fat, soft tissues) can be performed in this way [29]. Spectral differences between, for example, calcium and uric acid can be exploited to image gouty arthritis [30] (Fig. 2). DECT

techniques also allow separation of bone (i.e., calcium) signal from iodine so that bone segmentation can be performed without misregistration artifacts inherent when using separate mask acquisitions. Virtual unenhanced (VNC) datasets can be generated, saving radiation exposure associated with separate unenhanced CT acquisitions. A virtual monochromatic (VMC) dataset can be created, simulating the image quality obtained by a monochromatic x-ray beam. The CNR for iodine can be improved [31], and CT number calculations from VMC images have been shown to be significantly less variable than standard polychromatic images [32]. These techniques are depicted in Figure 3. DECT techniques have utility in many areas of diagnostic imaging, including CT urography, musculoskeletal imaging, and oncologic imaging (detection and characterization) [33], as well as CTA evaluation of gastrointestinal bleeding [34] and aortic endografts [35].

DECT techniques have several limitations. DSCT scanners used for dual-energy acquisitions have effective FOV limitations of 26–35 cm depending on scanner generation. Attention to positioning of the important anatomy within this FOV is very im-

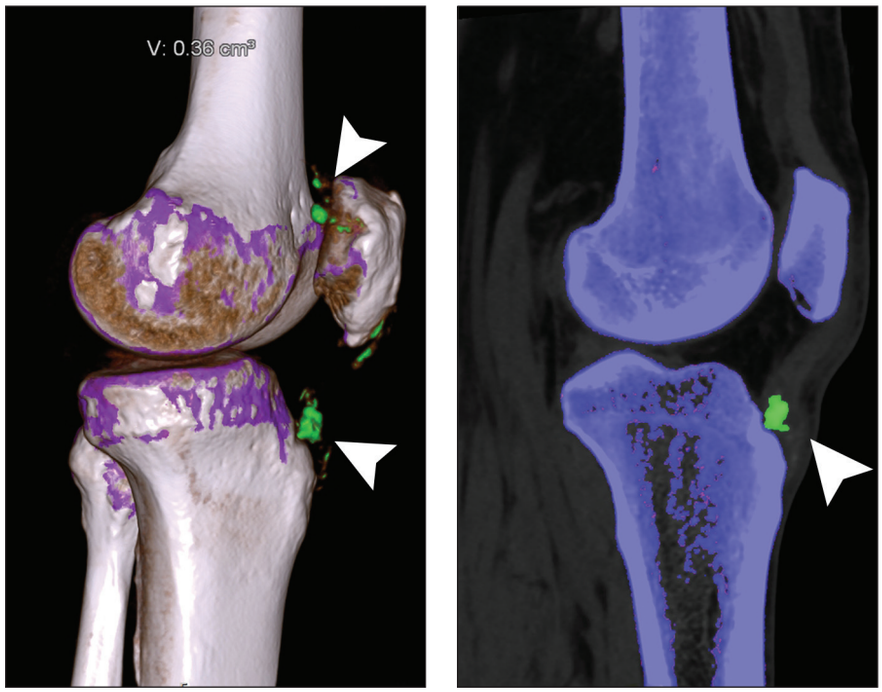

Fig. 2—Dual-energy CT discrimination of findings in setting of gout in patient who presented with knee pain.
A, Volume-rendered CT image with superimposed dual-energy data shows foci of uric acid crystals (*green*) in patellar tendon and suprapatellar bursal fluid (*arrowheads*). V = volume of urate deposits.
B, Sagittal CT reformation image with overlaid dual-energy signal shows material difference between urate deposits of tophaceous gout (*arrowhead*), depicted in green, and calcium in surrounding bony structures, depicted by purple.

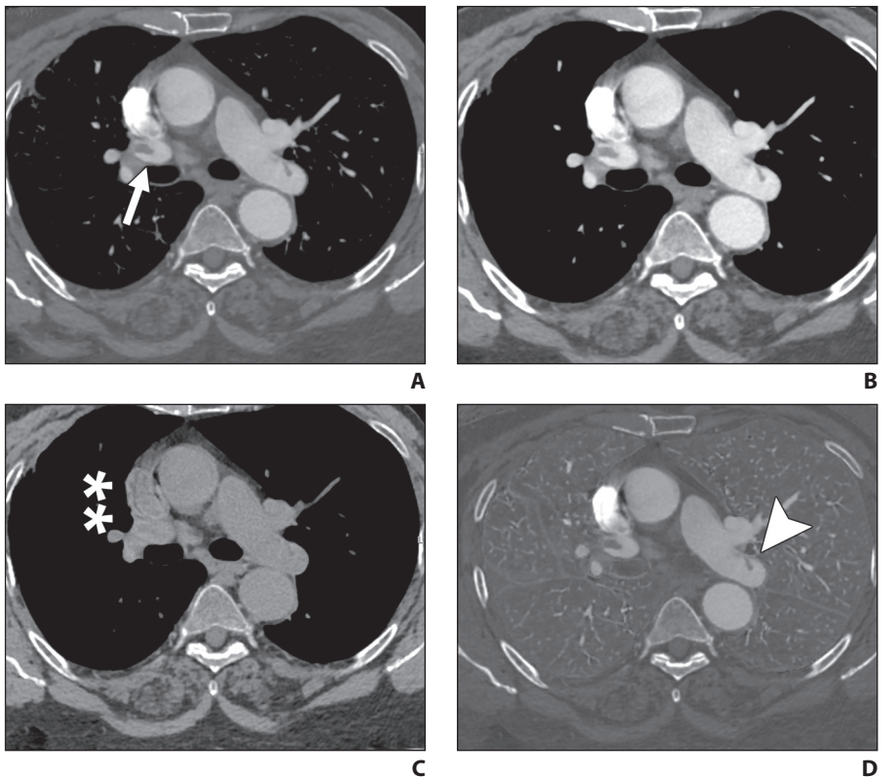

Fig. 3—Dual-energy CT (DECT) evaluation of pulmonary embolus in 75-year-old woman with history of breast cancer and previous deep venous thrombosis who presented with intermittent chest pain.
A, Virtual monoenergetic image. Note clarity of right upper lobe pulmonary embolus (*arrow*).
B, Nonlinear blended CT image approximating typical polychromatic 120-kVp image.
C, Virtual unenhanced image. Note near-complete iodine subtraction from superior vena cava and adjacent pulmonary artery (*asterisks*); however, clot can be faintly appreciated.
D, Iodine map image. Note clarity of weblike, nonocclusive defect (*arrowhead*) from chronic embolic disease.

portant (Fig. 4). Fast tube voltage-switching scanners do not offer patient-size automated exposure control adjustments and limit acquisition methods to a single milliampere value for the entire examination. Photon-starvation and beam-hardening artifacts are more pronounced with DECT techniques, especially in large patients, patients imaged with their arms at their sides, and patients with metallic implants. Increasing the low-energy tube voltage to 100 kVp instead of 80 kVp [36], reconstruction of high-kilo-

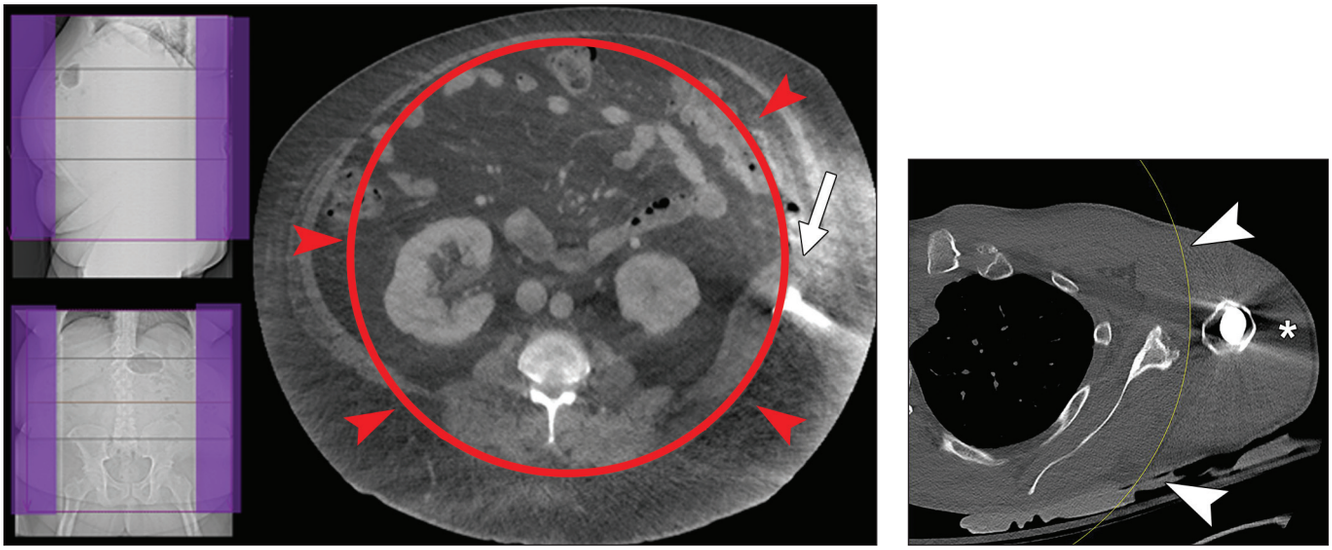

A B

Fig. 4—FOV considerations for dual-source CT (DSCT) acquisitions.
A, DSCT evaluation of patient who is obese (body mass index = 45). FOV limitations (33 cm) of second dual-source x-ray tube can be seen in purple on topogram images (*left*). Horizontal lines on topogram images show start and stop positions for scan (*top* and *bottom lines*) and level of axial image (*middle line*). DSCT image (*right*) shows that indwelling abscess drainage catheter (*arrow*) lies outside FOV (*arrowheads* and *circle*) and cannot be adequately assessed.
B, Patient with left shoulder prosthesis who presented for DSCT evaluation of bone-prosthesis interface. Anatomy in question is not centered in CT gantry, so prosthesis (*asterisk*) is outside FOV for dual-energy acquisition (*arrowheads* and *curved line*).

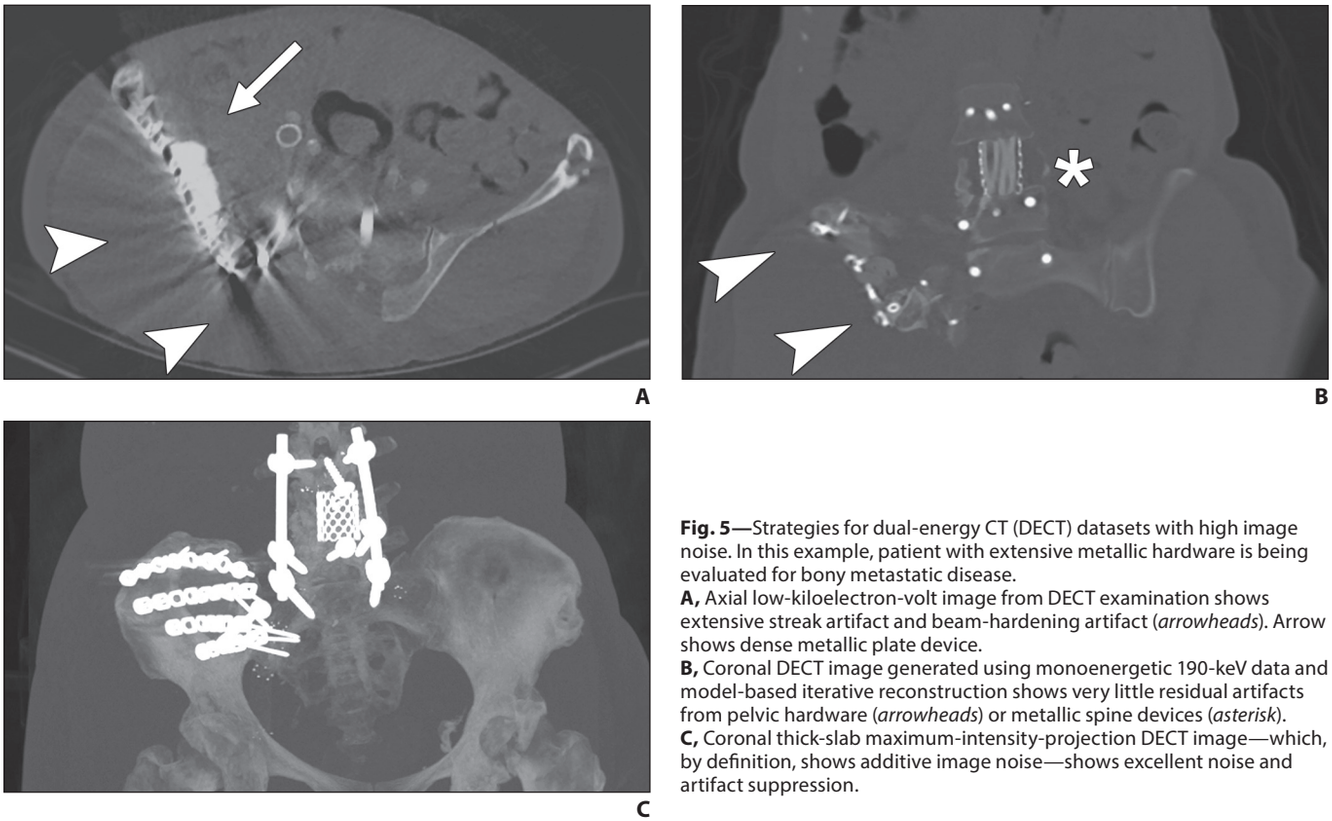

A B C

Fig. 5—Strategies for dual-energy CT (DECT) datasets with high image noise. In this example, patient with extensive metallic hardware is being evaluated for bony metastatic disease.
A, Axial low-kiloelectron-volt image from DECT examination shows extensive streak artifact and beam-hardening artifact (*arrowheads*). Arrow shows dense metallic plate device.
B, Coronal DECT image generated using monoenergetic 190-keV data and model-based iterative reconstruction shows very little residual artifacts from pelvic hardware (*arrowheads*) or metallic spine devices (*asterisk*).
C, Coronal thick-slab maximum-intensity-projection DECT image—which, by definition, shows additive image noise—shows excellent noise and artifact suppression.

electron-volt monoenergetic datasets [37] (Fig. 5), use of a tin (Sn) filter in front of the high-energy beam to improve spectral separation [38], and use of metallic artifact reduction reconstruction algorithms are a few of the available mechanisms to offset these limitations. Additionally, VNC images often show higher image noise, which is related to the addition of systematic noise from the decomposition algorithm [39], and may show incomplete iodine subtraction in the setting of a very high degree of contrast enhancement.

DECT techniques that remove calcium, iodine, or both work best when both materials are very dense. In situations in which the density of the material is low (e.g., bone marrow, small lesions with partial volume effect), results are not as satisfying [40]. Given that gradient-based segmentation techniques already in use perform reasonably well when contrast is high, DECT techniques may not add a large amount of incremental information in these particular situations.

Image Quality Assessment for New Protocols

When assessing the image quality of any new imaging or contrast parameter, it is important to not blindly rely on SNR measurements or subjective scores and instead to find a measurable parameter that reflects the clinical task demanded by CTA. For example, a meaningful parameter to compare a new technique for the evaluation of CTA before transcatheter aortic valve replacement would be the measurement reproducibility of the aortic annulus and access vessel diameters rather than SNR or subjective (e.g., diagnostic or not diagnostic) image quality.

Conclusion

Reliable, rational cardiovascular CT requires knowledge of early IV CM dynamics and manipulation of available CT scanner resources to create optimal injection and acquisition protocols. Current-generation CT technology allows rapid image acquisition. Therefore, the use of constant image acquisition times and CM injection duration will allow consistent high-quality CTA acquisition with the only variation in technique being related to customized injection flow rates (CM volumes) related to patient size. Clinical scanners also allow the use of low-tube-voltage imaging, which can be exploited to decrease radiation dose and potentially reduce necessary CM volume, related to improved attenuation of iodine. Options for DECT and DSCT are currently available from all major CT vendors. DSCT and DECT scanners can be used to acquire and process DECT datasets, including VNC and VMC images, which can be used to decrease radiation exposure and improve iodine visualization and pathologic characterization. Photon-counting CT can further expand and refine photon-energy discrimination and provide further noise rejection and reduction capability; it is likely that future refinements in scanner hardware will allow clinical implementation. By understanding the mechanisms of CM dynamics and scan acquisition, these newer techniques can be leveraged to provide enhanced patient care.

REFERENCES

1. Napel S, Marks MP, Rubin GD, et al. CT angiography with spiral CT and maximum intensity projection. *Radiology* 1992; 185:607–610
2. Fleischmann D, Boas FE. Computed tomography: old ideas and new technology. *Eur Radiol* 2011; 21:510–517
3. Hopper KD. With helical CT, is nonionic contrast a better choice than ionic contrast for rapid and large IV bolus injections? *AJR* 1996; 166:715–715
4. Katayama H, Yamaguchi K, Kozuka T, et al. Adverse reactions to ionic and nonionic contrast media: a report from the Japanese Committee on the Safety of Contrast Media. *Radiology* 1990; 175:621–628
5. Fleischmann D. Present and future trends in multiple detector-row CT applications: CT angiography. *Eur Radiol* 2002; 12(suppl 2):S11–S16
6. Fleischmann D, Rubin GD, Bankier AA, Hittmair K. Improved uniformity of aortic enhancement with customized contrast medium injection protocols at CT angiography. *Radiology* 2000; 214:363–371
7. Sheiman RG, Raptopoulos V, Caruso P, et al. Comparison of tailored and empiric scan delays for CT angiography of the abdomen. *AJR* 1996; 167:725–729
8. Hittmair K, Fleischmann D. Accuracy of predicting and controlling time-dependent aortic enhancement from a test bolus injection. *J Comput Assist Tomogr* 2001; 25:287–294
9. Bae KT, Heiken JP, Brink JA. Aortic and hepatic contrast medium enhancement at CT. Part II. Effect of reduced cardiac output in a porcine model. *Radiology* 1998; 207:657–662
10. Dawson P, Blomley MJ. Contrast media as extracellular fluid space markers: adaptation of the central volume theorem. *Br J Radiol* 1996; 69:717–722
11. Gosselin MV, Rassner UA, Thieszen SL, et al. Contrast dynamics during CT pulmonary angiogram: analysis of an inspiration associated artifact. *J Thorac Imaging* 2004; 19:1–7
12. Henk CB, Grampp S, Linnau KF, et al. Suspected pulmonary embolism: enhancement of pulmonary arteries at deep-inspiration CT angiography—influence of patent foramen ovale and atrial-septal defect. *Radiology* 2003; 226:749–755
13. Rubin GD. Three-dimensional helical CT angiography. *RadioGraphics* 1994; 14:905–912
14. Fleischmann D, Rubin GD. Quantification of intravenously administered contrast medium transit through the peripheral arteries: implications for CT angiography. *Radiology* 2005; 236:1076–1082
15. Fleischmann D, Chin AS, Molvin L, et al. Computed tomography angiography: a review and technical update. *Radiol Clin North Am* 2016; 54:1–12
16. Waaijer A, Prokop M, Velthuis BK, et al. Circle of Willis at CT angiography: dose reduction and image quality—reducing tube voltage and increasing tube current settings. *Radiology* 2007; 242:832–839
17. Padole A, Ali Khawaja RD, Kalra MK, Singh S. CT radiation dose and iterative reconstruction techniques. *AJR* 2015; 204:[web]W384–W392
18. Olcott EW, Shin LK, Sommer G, et al. Model-based iterative reconstruction compared to adaptive statistical iterative reconstruction and filtered backprojection in CT of the kidneys and the adjacent retroperitoneum. *Acad Radiol* 2014; 21:774–784
19. Yu L, Fletcher JG, Grant KL, et al. Automatic selection of tube potential for radiation dose reduction in vascular and contrast-enhanced abdominopelvic CT. *AJR* 2013; 201:[web]W297–W306
20. Baker ME, Karim W, Bullen JA, et al. Estimated patient dose indexes in adult and pediatric MDCT: comparison of automatic tube voltage selection with fixed tube current, fixed tube voltage, and weight-based protocols. *AJR* 2015; 205:592–598
21. Liang J, Wang H, Xu L, et al. Diagnostic performance of 256-row detector coronary CT angiography in patients with high heart rates within a single cardiac cycle: a preliminary study. *Clin Radiol* 2017; 72:694.e7–694.e14
22. Oh LC, Lau KK, Devapalasundaram A, et al. Efficacy of 'fine' focal spot imaging in CT abdominal angiography. *Eur Radiol* 2014; 24:3010–3016
23. Megibow AJ, Kambadakone A, Ananthakrishnan L. Dual-energy computed tomography: image acquisition, processing, and workflow. *Radiol Clin North Am* 2018; 56:507–520
24. Flohr TG, McCollough CH, Bruder H, et al. First performance evaluation of a dual-source CT (DSCT) system. *Eur Radiol* 2006; 16:256–268
25. Johnson TR. Dual-energy CT: general principles. *AJR* 2012; 199:(suppl 5)S3–S8
26. McCollough CH, Leng S, Yu L, Fletcher JG. Dual- and multi-energy CT: principles, technical approaches, and clinical applications. *Radiology* 2015; 276:637–653
27. Taguchi K, Frey EC, Wang X, et al. An analytical model of the effects of pulse pileup on the energy spectrum recorded by energy resolved photon counting x-ray detectors. *Med Phys* 2010; 37:3957–3969
28. Koenig T, Schulze J, Zuber M, et al. Imaging properties of small-pixel spectroscopic x-ray detectors based on cadmium telluride sensors. *Phys Med Biol* 2012; 57:6743–6759
29. Johnson TR, Krauss B, Sedlmair M, et al. Material differentiation by dual energy CT: initial experience. *Eur Radiol* 2007; 17:1510–1517
30. Desai MA, Peterson JJ, Garner HW, Kransdorf MJ. Clinical utility of dual-energy CT for evaluation of tophaceous gout. *RadioGraphics* 2011; 31:1365–1375; discussion, 1376–1377
31. Grant KL, Flohr TG, Krauss B, et al. Assessment of an advanced image-based technique to calculate virtual monoenergetic computed tomographic images from a dual-energy examination to im-

prove contrast-to-noise ratio in examinations using iodinated contrast media. *Invest Radiol* 2014; 49:586–592
32. Michalak G, Grimes J, Fletcher J, et al. Technical note: improved CT number stability across patient size using dual-energy CT virtual monoenergetic imaging. *Med Phys* 2016; 43:513–517
33. Agrawal MD, Pinho DF, Kulkarni NM, et al. Oncologic applications of dual-energy CT in the abdomen. *RadioGraphics* 2014; 34:589–612
34. Sun H, Hou XY, Xue HD, et al. Dual-source dual-energy CT angiography with virtual non-enhanced images and iodine map for active gastrointestinal bleeding: image quality, radiation dose and diagnostic performance. *Eur J Radiol* 2015; 84:884–891
35. Chandarana H, Godoy MC, Vlahos I, et al. Abdominal aorta: evaluation with dual-source dual-energy multidetector CT after endovascular repair of aneurysms—initial observations. *Radiology* 2008; 249:692–700
36. Wortman JR, Uyeda JW, Fulwadhva UP, Sodickson AD. Dual-energy CT for abdominal and pelvic trauma. *RadioGraphics* 2018; 38:586–602
37. Lewis M, Reid K, Toms AP. Reducing the effects of metal artefact using high keV monoenergetic reconstruction of dual energy CT (DECT) in hip replacements. *Skeletal Radiol* 2013; 42:275–282
38. Krauss B, Grant KL, Schmidt BT, Flohr TG. The importance of spectral separation: an assessment of dual-energy spectral separation for quantitative ability and dose efficiency. *Invest Radiol* 2015; 50:114–118
39. Altenbernd J, Heusner TA, Ringelstein A, et al. Dual-energy-CT of hypervascular liver lesions in patients with HCC: investigation of image quality and sensitivity. *Eur Radiol* 2011; 21:738–743
40. Tran DN, Straka M, Roos JE, et al. Dual-energy CT discrimination of iodine and calcium: experimental results and implications for lower extremity CT angiography. *Acad Radiol* 2009; 16:160–171